

Graph VQ-Transformer (GVT): Fast and Accurate Molecular Generation via High-Fidelity Discrete Latents

Haozhuo Zheng, Cheng Wang, Yang Liu*

Harbin Institute of Technology
24B903065@stu.hit.edu.cn, 21S003047@stu.hit.edu.cn, liuyang@hit.edu.cn

Abstract

The *de novo* generation of molecules with desirable properties is a critical challenge, where diffusion models are computationally intensive and autoregressive models struggle with error propagation. In this work, we introduce the Graph VQ-Transformer (GVT), a two-stage generative framework that achieves both high accuracy and efficiency. The core of our approach is a novel Graph Vector Quantized Variational Autoencoder (VQ-VAE) that compresses molecular graphs into high-fidelity discrete latent sequences. By synergistically combining a Graph Transformer with canonical Reverse Cuthill-McKee (RCM) node ordering and Rotary Positional Embeddings (RoPE), our VQ-VAE achieves near-perfect reconstruction rates. An autoregressive Transformer is then trained on these discrete latents, effectively converting graph generation into a well-structured sequence modeling problem. Crucially, this mapping of complex graphs to high-fidelity discrete sequences bridges molecular design with the powerful paradigm of large-scale sequence modeling, unlocking potential synergies with Large Language Models (LLMs). Extensive experiments show that GVT achieves state-of-the-art or highly competitive performance across major benchmarks like ZINC250k, MOSES, and GuacaMol, and notably outperforms leading diffusion models on key distribution similarity metrics such as FCD and KL Divergence. With its superior performance, efficiency, and architectural novelty, GVT not only presents a compelling alternative to diffusion models but also establishes a strong new baseline for the field, paving the way for future research in discrete latent-space molecular generation.

Code — <https://github.com/zzccppp/GVT.git>

Introduction

The *de novo* generation of molecular graphs with desired chemical and physical properties is a cornerstone of modern drug discovery, materials science, and chemical engineering (Jin, Barzilay, and Jaakkola 2018; Faez et al. 2021). Molecules are naturally represented as graphs, with atoms as nodes and bonds as edges. These graphs are governed by complex topological features and strict chemical valency rules. Developing generative models that can effectively navigate this intricate chemical space to produce valid,

novel, and useful molecules remains a formidable scientific challenge.

Various deep learning paradigms have been applied to this task. While early approaches included Generative Adversarial Networks (GANs) (De Cao and Kipf 2018) and Variational Autoencoders (VAEs) (Simonovsky and Komodakis 2018), score-based diffusion models have recently set a high standard for generation quality (Niu et al. 2020; Jo, Lee, and Hwang 2022; Yan et al. 2023). However, their iterative sampling process often incurs significant computational overhead and handles the discrete constraints of molecular structures only indirectly. Even hybrid methods aiming to improve this, like PARD (Zhao, Ding, and Akoglu 2024), which combines diffusion with an autoregressive model, introduces significant framework complexity and still faces challenges with sampling speed. Another prominent approach, Autoregressive (AR) graph generation (You et al. 2018; Jin, Barzilay, and Jaakkola 2018), constructs graphs sequentially. While intuitive, direct AR methods often suffer from error accumulation and struggle to enforce global chemical validity without complex, hard-coded rules.

Prior work has also explored two-stage generative frameworks that combines discrete latent representations with autoregressive sequence modeling. For instance, DGAE (Bogget, Gregorova, and Kalousis 2023) investigated a Graph VQ-VAE with an autoregressive component for molecular generation. While promising in their conceptualization, such discrete latent-based approaches have not consistently surpassed the performance of diffusion models, particularly in terms of generation quality and diversity, nor have they fully addressed the limitations of enforcing chemical rules implicitly.

This work introduces Graph VQ-Transformer (GVT), a two-stage framework that leverages the strengths of high-fidelity discrete latent representations and powerful Transformer-based sequence modeling. GVT pushes the boundaries of what two-stage generative models can achieve in molecular design, offering a compelling alternative to computationally intensive continuous diffusion models. Our contributions are:

- We design a novel Graph Vector Quantized Variational Autoencoder (VQ-VAE) that achieves exceptionally high reconstruction fidelity on complex molecular datasets. This effectively solves the fidelity bottleneck that limits

*Corresponding author.

previous two-stage models.

- At the core of our VQ-VAE is a new decoder architecture that synergistically combines Reverse Cuthill-McKee (RCM) for canonical node ordering with a Graph Transformer enhanced by Rotary Positional Encodings (RoPE). This mechanism is crucial, as it allows the decoder to interpret sequential proximity in the latent space as structural information, resolving ambiguities that standard GNNs cannot.
- We demonstrate that GVT’s high-fidelity latents translate directly to state-of-the-art generative performance. Our full model achieves superior or highly competitive results across major benchmarks, significantly outperforming leading diffusion models on key distribution similarity metrics and presenting a fast, accurate alternative for molecular design.

We empirically validate GVT on the QM9(Wu et al. 2018), ZINC250k(Irwin et al. 2012), MOSES(Polykovskiy et al. 2020), and GuacaMol(Brown et al. 2019) datasets, showing its effectiveness for both high-fidelity representation learning and efficient, high-quality molecular generation.

Related Work

Autoregressive Graph Generation

Autoregressive (AR) models have been widely adapted for discrete graph structures, typically by constructing a graph step-by-step. This sequential approach inherently acknowledges the discrete nature of graphs but faces a key challenge: graphs lack a single, canonical order for their nodes and edges. The performance of an AR model thus depends heavily on the ordering scheme used to serialize the graph, as it aims to model the probability $p(G) = \sum_{\pi \in \mathcal{P}(G)} p(G, \pi)$ over all possible permutations.

To address this, early AR graph generation models focused on defining a canonical ordering for the nodes before generation. Pioneering works like GraphRNN (You et al. 2018) and GRAN (Liao et al. 2019) proposed various strategies, such as using Breadth-First Search (BFS) or sorting nodes by their degree, to create a consistent sequence from a graph structure. These methods aim to transform the complex graph generation task into a more manageable sequential prediction problem.

In a two-stage framework like ours, this principle of ordering is even more critical. Our AR model does not operate on the graph directly, but on a sequence of discrete latent codes produced by the VQ-VAE encoder. Therefore, a consistent and structurally meaningful node ordering is paramount. It ensures that the resulting latent sequence is predictable and that the AR model can effectively learn local dependencies, as structurally adjacent nodes in the graph are mapped to nearby positions in the latent sequence. This stable mapping is the foundation upon which our high-performing generative model is built.

Graph Autoencoders and Vector Quantization

Graph autoencoders (GAEs) are crucial for learning low-dimensional latent representations for generation. Early

methods used a single, continuous, graph-level vector (Simonovsky and Komodakis 2018), but this approach struggled with complex and inaccurate reconstruction. To simplify this, subsequent work shifted to node-level continuous latent spaces (Samanta et al. 2020; Li, Zhang, and Liu 2018), but this introduced latent-node collapse, where embeddings become indistinguishable and fail to capture local structure.

To solve this, recent efforts have turned to discrete latent spaces using Vector Quantization (VQ), as popularized by VQ-VAEs (Oord, Vinyals, and Kavukcuoglu 2018) and adapted for graph data (Yang et al. 2023). VQ maps continuous vectors to a finite, learned codebook, creating a more structured representation. However, prior Graph VQ-VAE models like DGAE (Boget, Gregorova, and Kalousis 2023) were limited by low reconstruction fidelity. A generative model trained on such noisy discrete codes cannot be expected to master complex chemical rules. This analysis motivates our central focus: developing a Graph VQ-VAE capable of exceptionally high-fidelity reconstruction, thereby providing a robust foundation for the subsequent autoregressive model.

Methods

Our proposed framework, illustrated in Figure 1, consists of two main stages: (1) learning high-fidelity discrete representations of molecules using a novel Graph VQ-VAE, and (2) training an autoregressive model on these discrete sequences.

Stage 1: High-Fidelity Discrete Molecular Representation with Graph VQ-VAE

The first stage of our framework is to learn a mapping from a molecular graph $\mathbf{G} = (\mathbf{X} \in \mathbb{R}^{N \times d_x}, \mathbf{E} \in \mathbb{R}^{N \times N \times d_e})$ to a sequence of discrete integer codes $K = (k_1, k_2, \dots, k_N)$, from which \mathbf{G} can be perfectly reconstructed. The success of the entire generative pipeline hinges on the fidelity of this stage. Our design is motivated by solving key challenges inherent in graph representation.

The Challenge: Structural Ambiguity and Permutation Equivariance A core property of Graph Neural Networks (GNNs) is permutation equivariance. While powerful, this property creates a challenge for reconstruction: a standard GNN decoder treats structurally identical nodes as indistinguishable. This ambiguity can make it difficult for the decoder to precisely reconstruct specific bond connections, as it lacks a mechanism to differentiate between these symmetric nodes.

To illustrate this challenge with a concrete, empirically observed example, consider the example molecule from the GuacaMol dataset shown in Figure 2. After passing through our VQ-VAE encoder, several atoms are mapped to their corresponding discrete codebook indices (k_i). Notably, three distinct oxygen atoms, each double-bonded to a carbon atom within a carboxyl group, are all mapped to the identical codebook index, $k = 211$.

For a standard, permutation-equivariant GNN decoder, these three nodes are indistinguishable. They possess identical feature information (the latent code for $k = 211$) and,

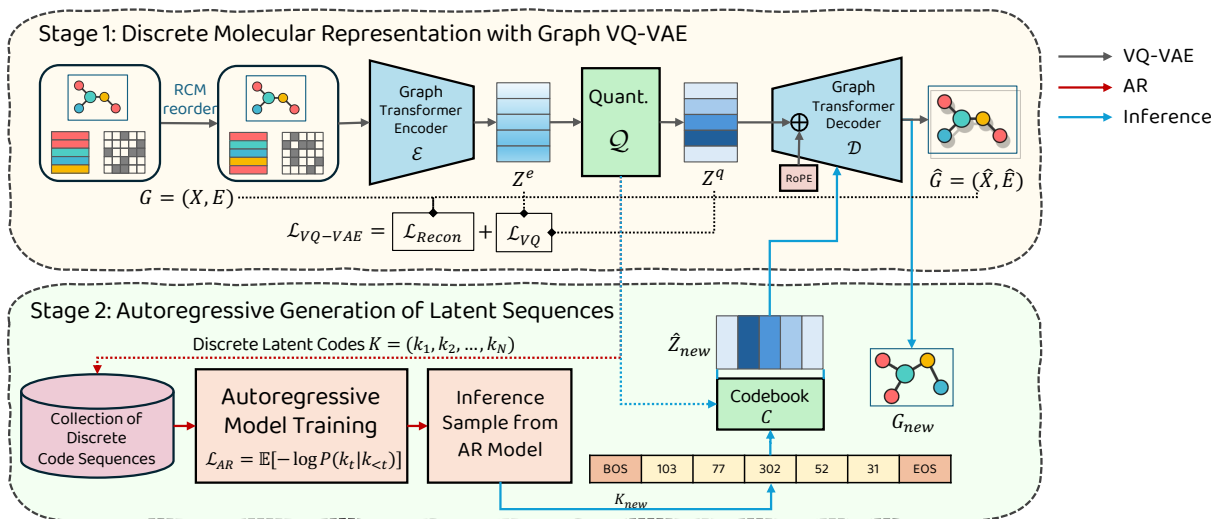


Figure 1: An overview of our proposed two-stage framework. **Stage 1: Graph VQ-VAE.** A molecular graph is first preprocessed with Reverse Cuthill-McKee (RCM) for canonical node ordering. The Graph Transformer-based Encoder maps the graph to continuous latent vectors, which are then quantized into a sequence of discrete codes by the Vector Quantization (VQ) layer. The Decoder, which uniquely uses RoPE to interpret sequential proximity as structural information, reconstructs the graph from these codes. The model is trained end-to-end via a reconstruction and commitment loss. **Stage 2: Autoregressive Generation.** The trained VQ-VAE is used to encode a dataset of molecules into discrete latent sequences. A decoder-only autoregressive Transformer is then trained on these sequences. New molecules are generated by sampling a latent sequence from the AR model and decoding it back into a graph using the pre-trained VQ-VAE decoder.

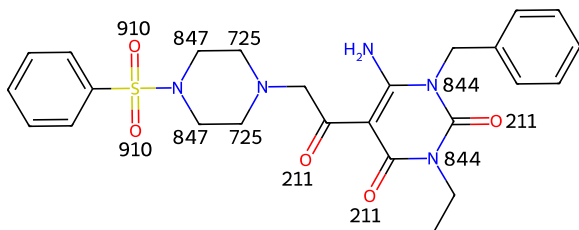


Figure 2: An example of structural ambiguity. Three distinct oxygen atoms are encoded into the same discrete latent code ($k = 211$).

within the assumed fully-connected latent graph that the decoder operates on, they hold equivalent topological status. This creates a critical ambiguity: the decoder has no intrinsic information to correctly associate each oxygen with its specific parent carbon atom. It might erroneously attempt to connect one carbon to multiple oxygens, or vice-versa, leading to invalid chemical structures during reconstruction.

Canonical Node Ordering with Reverse Cuthill-McKee (RCM) To resolve this ambiguity, we first establish a consistent, structurally-aware node sequence for every graph. We preprocess all input graphs using the Reverse Cuthill-McKee (RCM) algorithm (Cuthill and McKee 1969), which reorders nodes to minimize the bandwidth of the adjacency

matrix. This canonicalization ensures that structurally proximal nodes are placed close to each other in the sequence, providing a deterministic order that breaks symmetries. Our choice of RCM is empirically validated against other common ordering schemes like Breadth-First Search (BFS) and random ordering, as detailed in the Appendix, where RCM consistently yields the highest reconstruction fidelity. However, this introduces a new challenge: a standard GNN decoder, by its equivariant nature, is designed to ignore this valuable ordering information. Simply feeding it an ordered sequence would be futile.

Encoder \mathcal{E} The encoder \mathcal{E} maps an RCM-ordered input graph \mathbf{G} to a set of node-level continuous latent vectors $\mathbf{Z}^e = \{\mathbf{z}_i^e\}_{i=1}^N$, where $\mathbf{z}_i^e \in \mathbb{R}^{d_e}$. Input node features \mathbf{X} , edge features \mathbf{E} , and Laplacian Positional Encodings \mathbf{P} are processed through L_{enc} layers of a Graph Transformer network (Yun et al. 2019). The Graph Transformer layers update node and edge representations using attention mechanisms that integrate node, edge, and positional information:

$$(\mathbf{H}^{(l+1)}, \mathbf{E}^{(l+1)}) = \text{GTLayer}(\mathbf{H}^{(l)}, \mathbf{E}^{(l)}, \mathbf{P}, \mathbf{A})$$

After the final Graph Transformer layer, we obtain the node representations $\mathbf{H}^{(L_{enc})}$ and edge representations $\mathbf{E}^{(L_{enc})}$. To generate a more comprehensive node embedding, we introduce a fusion step that combines these two sources of information. Specifically, for each node i , we first aggregate the features of its incoming edges by computing their mean:

$$\mathbf{e}_i^{\text{agg}} = \text{mean}_{j:(j,i) \in \mathcal{E}} (\mathbf{e}_{ji}^{(L_{enc})})$$

where $\mathbf{e}_{ji}^{(L_{enc})}$ is the feature vector of the edge from node j to node i produced by the final layer, and \mathcal{E} is the set of edges in the graph. This aggregated edge information is then concatenated with the node’s own representation, $\mathbf{h}_i^{(L_{enc})} \in \mathbf{H}^{(L_{enc})}$. The resulting vector is passed through a final linear fusion layer to produce the final node latent vector \mathbf{z}_i^e :

$$\mathbf{z}_i^e = \mathbf{W}_f \left(\mathbf{h}_i^{(L_{enc})} \parallel \mathbf{e}_i^{\text{agg}} \right) + \mathbf{b}_f$$

where \mathbf{W}_f and \mathbf{b}_f are the trainable weight matrix and bias of the linear fusion layer, and \parallel denotes the concatenation operation. The complete set of these vectors $\mathbf{Z}^e = \{\mathbf{z}_i^e\}_{i=1}^N$ constitutes the output of the encoder. This entire encoder architecture, including the fusion stage, is permutation equivariant.

Vector Quantization Layer \mathcal{Q} The continuous latent vectors \mathbf{Z}^e are mapped to discrete representations using a standard Vector Quantization (VQ) layer. A learnable codebook $\mathbf{C} = \{\mathbf{c}_k\}_{k=1}^{K_c}$ contains K_c codebook vectors (embeddings) of dimension d_c . Each \mathbf{z}_i^e is mapped to its closest codebook vector \mathbf{c}_{k_i} :

$$k_i = \arg \min_k \|\mathbf{z}_i^e - \mathbf{c}_k\|_2^2$$

To enable end-to-end training through this non-differentiable operation, the gradient from the quantized vectors \mathbf{Z}_q is copied directly to the encoder’s output \mathbf{Z}^e during the backward pass using a straight-through estimator. The output is a sequence of quantized vectors $\mathbf{Z}^q = \{\mathbf{z}_i^q\}_{i=1}^N$ where $\mathbf{z}_i^q = \mathbf{c}_{k_i}$, and the corresponding integer indices $K = (k_1, \dots, k_N)$.

Decoder \mathcal{D} : Fusing Order and Structure with RoPE Our decoder is specifically designed to bridge the gap between the RCM-imposed node order and the need for structural reconstruction. To achieve this, we employ a Graph Transformer architecture uniquely enhanced with Rotary Position Embeddings (RoPE) (Su et al. 2024). This is the core of our VQ-VAE’s high fidelity. The synergy is twofold: RCM embeds structural proximity into sequential proximity, and RoPE allows the attention mechanism to directly process this sequential information as a relative positional signal.

The reconstruction process proceeds in two steps:

1. **Injecting Relative Positional Awareness via RoPE:** We first transform the raw sequence of quantized vectors \mathbf{Z}^q into a position-aware sequence $\mathbf{Z}^{q'}$. RoPE achieves this by rotating each vector \mathbf{z}_i^q based on its absolute position i . The critical property of RoPE is that the subsequent attention score between any two vectors at positions i and j becomes an elegant function of their content and their relative distance, $i-j$. Since RCM ordering ensures that a small relative distance implies structural closeness, RoPE provides the decoder with a direct and powerful signal for graph topology. This position-aware sequence $\mathbf{Z}^{q'}$ serves as the initial node representations $\mathbf{H}^{(0)}$ for the decoder.
2. **Iterative Graph Reconstruction:** With position-aware node embeddings $\mathbf{H}^{(0)}$, the Graph Transformer decoder iteratively refines the graph structure. First, initial edge features $\mathbf{E}^{(0)}$ are predicted by a shared MLP

that processes pairs of node embeddings, ensuring symmetry. These initial predictions, along with $\mathbf{H}^{(0)}$, are fed into a stack of L_{dec} Graph Transformer layers. Each layer updates both node and edge representations: $(\mathbf{H}^{(l+1)}, \mathbf{E}^{(l+1)}) = \text{GTLayer}(\mathbf{H}^{(l)}, \mathbf{E}^{(l)})$. After the final layer, the node representations $\mathbf{H}^{(L_{dec})}$ become the reconstructed node features $\hat{\mathbf{X}}$, and the final edge representations $\mathbf{E}^{(L_{dec})}$ are symmetrized to form the reconstructed adjacency and edge-type matrix $\hat{\mathbf{A}}$.

This design allows the decoder to leverage the canonical ordering effectively, leading to highly accurate graph reconstruction.

VQ-VAE Training The VQ-VAE is trained end-to-end by minimizing a combined loss function, which includes reconstruction terms for node and edge features, as well as the standard VQ commitment loss:

$$\mathcal{L}_{\text{VQ-VAE}} = \lambda_{\text{node}} \mathcal{L}_{\text{node}} + \lambda_{\text{edge}} \mathcal{L}_{\text{edge}} + \|\text{sg}(\mathbf{Z}^e) - \mathbf{Z}^q\|_2^2 + \beta \|\mathbf{Z}^e - \text{sg}(\mathbf{Z}^q)\|_2^2 \quad (1)$$

Here, $\mathcal{L}_{\text{node}}$ and $\mathcal{L}_{\text{edge}}$ are cross-entropy losses for reconstruction. The latter two terms align the encoder output with the codebook, where $\text{sg}(\cdot)$ is the stop-gradient operator. A detailed summary of the two-stage training procedure is provided as pseudocode in the Appendix.

Stage 2: Autoregressive Generation of Latent Sequences

Once the Graph VQ-VAE is trained, its encoder \mathcal{E} and quantizer \mathcal{Q} are used to convert a dataset of RCM-ordered molecular graphs into their corresponding sequences of discrete latent codes $K = (k_1, k_2, \dots, k_N)$.

We then train a Transformer-based decoder-only autoregressive model (similar to GPT2 (Radford et al. 2019)) to model the distribution $P(K)$. The model predicts the next code k_t given the previous codes $k_{<t}$:

$$P(K) = \prod_{t=1}^N P(k_t | k_{<t}; \theta_{AR})$$

The AR model is trained by minimizing the negative log-likelihood (cross-entropy loss) of the true sequences:

$$\mathcal{L}_{AR} = - \sum_{\text{seq } K} \sum_{t=1}^N \log P(k_t | k_{<t}; \theta_{AR})$$

The RCM ordering provides a canonical and structurally relevant sequence for the AR model, simplifying the learning of dependencies, especially local connectivity patterns which are often reflected in nearby tokens.

Experiments

The Critical Role of RoPE in Reconstruction

Our central hypothesis is that near-perfect reconstruction is the cornerstone of a successful two-stage generative

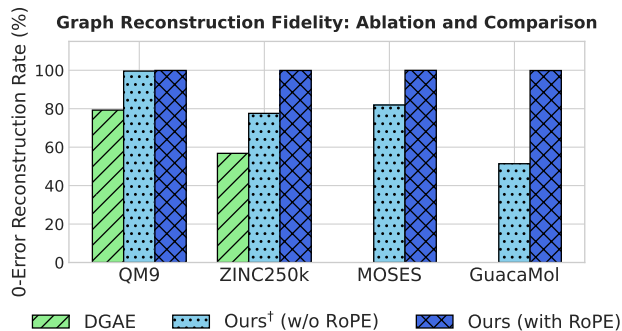


Figure 3: 0-Error Reconstruction Rate (%) on test sets. Our full model (GVT with RoPE) achieves near-perfect reconstruction, drastically outperforming both the previous DGAE’s GAE and our own architecture without the crucial RoPE component, especially on complex datasets.

model. A VQ-VAE that produces flawed latents cannot effectively teach a subsequent autoregressive model the complex rules of chemistry. To validate this and dissect our architectural contributions, we measure the 0-error reconstruction rate—the percentage of flawlessly rebuilt graphs—and present our findings in Figure 3.

Our results confirm this hypothesis in a step-by-step manner. First, the DGAE model validates the limitations of prior work, correctly reconstructing only 79.26% of QM9 and 56.78% of ZINC250k molecules. Our GVT architecture without RoPE already shows significant improvement (99.56% on QM9), but struggles with complex datasets like GuacaMol (51.38%), indicating that RCM ordering alone is insufficient. The critical role of RoPE is undeniable: activating it pushes the reconstruction rate to near-perfection across all benchmarks, including 99.89% on ZINC250k and 99.84% on GuacaMol. This dramatic leap, especially the over 48-point gain on GuacaMol, provides conclusive evidence that our synergistic design effectively solves the fidelity problem.

In summary, this analysis validates that our combination of a Graph Transformer, RCM ordering, and particularly RoPE, creates the high-fidelity discrete representations necessary for robust molecular generation. This solid foundation is what enables the success of our subsequent autoregressive model. In the Appendix, we further explore the impact of another key design choice, the codebook size, demonstrating its effect on reconstruction performance and training convergence.

Molecule Graph Generation

Datasets. We experiment with four different molecular datasets: QM9(Wu et al. 2018), ZINC250k(Irwin et al. 2012), MOSES(Polykovskiy et al. 2020), GuacaMol(Brown et al. 2019).

For experimental setup, we use a fixed 80%-20% training-test split for the QM9 and ZINC250k datasets. For MOSES and GuacaMol, we adhere to their officially defined data splits to ensure fair comparison with previous work. Fol-

lowing (Jo, Lee, and Hwang 2022), we remove hydrogen atoms and kekulize molecules by RDKit (Landrum et al. 2016). Detailed hyperparameters for our models, including layer counts, dimensions, and training configurations for each dataset, are provided in the Appendix.

Baselines. We benchmark our model against a diverse set of baselines from state-of-the-art graph generative model families. The specific models for comparison vary depending on the dataset and its standard evaluation protocol.

For QM9 and ZINC250k, we compare against a comprehensive suite of recent graph-native generative models. These are grouped into three main categories:

- **Flow-based Models:** This category includes generative flow models such as GraphAF (Shi et al. 2020) and GraphDF (Luo, Yan, and Ji 2021).
- **Diffusion Models:** We select a range of representative diffusion-based approaches, namely the score-based GDSS (Jo, Lee, and Hwang 2022), the discrete DiGress (Vignac et al. 2022), SwinGNN (Yan et al. 2023), and GLAD (Nguyen et al. 2025).
- **Hybrid Autoregressive Models:** In this category, we include DGAE (Boget, Gregorova, and Kalousis 2023), which is architecturally the most analogous to our approach as it also combines a VQ-VAE with an autoregressive (AR) framework. We also compare against PARD (Zhao, Ding, and Akoglu 2024), which represents a different hybrid strategy that integrates AR modeling with a diffusion backbone.

For the MOSES benchmark, in addition to recent one-shot methods like DiGress and PARD, we follow the standard protocol by also comparing against a wider array of established models. As shown in Table 2, this includes methods that operate on different molecular representations, such as SMILES-based VAEs, fragment-based models like JT-VAE, and the classic autoregressive model GraphINVENT.

For the GuacaMol benchmark, we compare against several models from its standard leaderboard to assess performance on goal-directed tasks. As shown in Table 3, these baselines include the SMILES-based LSTM, as well as one-shot methods like NAGVAE and the search-based MCTS.

Metrics. To comprehensively evaluate the performance of our model against baselines, we employ a set of widely-recognized metrics for molecular generation, sourced from standard benchmarks like GuacaMol (Brown et al. 2019) and MOSES (Polykovskiy et al. 2020). Core metrics include **Validity (Val.)**, the percentage of chemically valid molecules; **Uniqueness (Uni.)**, the proportion of unique structures among valid ones to detect mode collapse; and **Novelty**, the percentage of valid unique molecules not present in the training set. As explained in (Vignac et al. 2022), Novelty is not reported in main table. To assess distribution similarity, we use the **Fréchet ChemNet Distance (FCD)**, where a lower score indicates higher similarity. For a deeper structural comparison, we report the **Network-based Shortest Path Difference Kernel (NSPDK)**, where lower values are also better. The MOSES benchmark provides a more holistic suite, including **Scaffold Similarity (SNN)** and **Scaffold Uniqueness (Scaf)** for scaffold-level

Methods	Class	QM9				ZINC250k			
		Val. \uparrow	Uni. \uparrow	FCD \downarrow	NSPDK \downarrow	Val. \uparrow	Uni. \uparrow	FCD \downarrow	NSPDK \downarrow
GraphAF	Flow-Based	57.16	83.78	5.384	2.10e-2	68.47	99.01	16.023	4.40e-2
GraphDF		79.33	95.73	11.283	7.50e-2	41.84	93.75	40.51	3.54e-1
GDSS	Diffusion	90.36	94.70	2.923	4.40e-3	97.35	99.76	11.398	1.80e-2
DiGress		95.43	93.78	0.643	7.28e-4	84.94	99.21	4.88	8.75e-3
SwinGNN		99.68	95.92	0.169	4.02e-4	87.74	99.98	5.219	7.52e-3
GLAD		97.12	97.52	0.201	3e-4	81.81	100	2.54	2.00e-3
PARD	Hybrid	97.5	95.8	-	-	95.23	99.99	1.98	-
DGAE		92.0	97.61	0.86	1.50e-3	77.9	99.94	4.4	7.00e-3
Ours	VQVAE+AR	99.76	95.94	0.87	6.0e-4	99.57	97.55	1.16	6.89e-2

Table 1: QM9 and ZINC250k Generation Results.

Model	Class	Val. \uparrow	Unique \uparrow	Novel \uparrow	Filters \uparrow	FCD \downarrow	SNN \uparrow	Scaf \uparrow
VAE	SMILES	97.7	99.8	69.5	99.7	<u>0.57</u>	<u>0.58</u>	5.9
JT-VAE	Fragment	100	100	99.9	97.8	1.00	0.53	10
GraphINVENT	AR	96.4	99.8	-	95.0	1.22	0.54	12.7
ConGress	Diffusion	83.4	99.9	<u>96.4</u>	94.8	1.48	0.50	16.4
DiGress	Diffusion	85.7	100	95.0	97.1	1.19	0.52	<u>14.8</u>
PARD	AR+Diffusion	86.8	100	78.2	99.0	1.00	0.56	2.2
Ours	VQVAE+AR	<u>99.42</u>	100	61.43	<u>99.59</u>	0.16	0.64	3.4

Table 2: Molecule generation on MOSES. All metrics \uparrow except FCD \downarrow .

analysis, and a **Filters** metric which reports the percentage of molecules passing medicinal chemistry screens. The GuacaMol benchmark introduces a goal-directed **KL Divergence (KL div)** score, which measures the similarity of physicochemical property distributions, with higher scores indicating a better match.

Main Results

We present the generation results on QM9, ZINC250k, MOSES, and GuacaMol in Table 1, 2, and 3, respectively. For fair comparison, all baseline results reported in the tables are sourced from their original publications. The results demonstrate that our autoregressive model achieves highly competitive, and often state-of-the-art, performance, particularly on large and challenging benchmarks. Our approach consistently matches or exceeds the performance of leading diffusion models, traditional rule-based autoregressive methods, and SMILES-string-based models.

Performance on QM9 and ZINC250k. On the small QM9 dataset, our model achieves the highest validity (99.76%) among all baselines. More importantly, on the large-scale and more challenging ZINC250k benchmark, our model demonstrates its superiority in distribution learning. It achieves a state-of-the-art FCD score of 1.16, significantly outperforming all diffusion-based counterparts such as PARD (1.98) and GLAD (2.54). Furthermore, it attains the highest validity score of 99.38%, confirming its ability to learn robust chemical rules for complex molecules.

Performance on MOSES Benchmark. This strong performance continues on the MOSES benchmark, another large-scale dataset. As shown in Table 2, our model sets a new state-of-the-art in distribution similarity with an FCD score of 0.16, which is over 3 times better than the next best competitor (VAE, 0.57). It also achieves the highest diversity score (SNN of 0.64) and passes nearly all medicinal chemistry filters (99.59%). This result is particularly noteworthy as it surpasses not only other diffusion graph generation methods (e.g., DiGress), but also models that operate on different representations like SMILES strings (VAE) and fragments (JT-VAE).

Performance on GuacaMol Benchmark. On the GuacaMol distribution learning benchmark, GVT demonstrates state-of-the-art performance. As shown in Table 3, it achieves the highest KL Divergence score (99.61), significantly outperforming other graph-native models like NAG-VAE and MCTS that fail on this task despite high validity. Crucially, GVT also maintains a high FCD score (85.50), showcasing a holistic ability to replicate both the statistical (physicochemical) and structural properties of the target distribution, a feat not guaranteed by simpler 1D SMILES-based models.

Discussion on Model Limitations While GVT shows robust performance, we acknowledge two primary limitations inherent to its design, which highlight areas for future improvement.

First, on ZINC250k, GVT’s excellent FCD score con-

Model	Class	Valid \uparrow	Unique \uparrow	Novel \uparrow	KL div \uparrow	FCD \uparrow
LSTM	SMILES	95.9	100	91.2	<u>99.1</u>	91.3
NAGVAE	Autoregressive	92.9	95.5	100	38.4	0.9
MCTS	Search-based	100	100	95.4	82.2	1.5
DiGress	Diffusion	85.2	100	<u>99.9</u>	92.9	68.0
Ours	VQVAE+AR	<u>97.46</u>	<u>99.9</u>	82.39	99.61	<u>85.50</u>

Table 3: Molecule generation on GuacaMol. We report scores from benchmark, so that higher is better for all metrics.

trasts with a poorer NSPDK score compared to diffusion models. This suggests high fidelity in local chemical features but a mismatch in global graph topology. We attribute this to the model’s inherently local focus. The autoregressive generation of a token sequence, even one ordered by RCM, excels at predicting local connectivity but may not adequately enforce the global topological constraints measured by NSPDK—a task where holistic update models like diffusion may have an advantage.

Second, the lower Novelty scores on MOSES and GuacaMol reflect a deliberate design trade-off prioritizing distribution fidelity over generative exploration. GVT’s training objective, combining near-perfect reconstruction with maximum likelihood, incentivizes the model to master the training distribution. While this leads to state-of-the-art distribution-similarity scores (FCD/KL-Div), it naturally reduces the likelihood of generating highly novel scaffolds from the low-probability tails of the learned distribution. However, this limitation is partially offset by GVT’s high sampling efficiency. Its fast generation speed allows for extensive over-sampling, where generating a vast number of candidates in a short time significantly increases the chance of discovering unique and novel structures, a practical remedy not always feasible for slower models. Furthermore, as demonstrated in the Appendix, the novelty can be substantially improved by adjusting sampling parameters like temperature and top-k, which encourages the model to explore less probable regions of the latent space without a significant drop in validity.

In summary, across multiple challenging benchmarks, our autoregressive model proves to be a powerful and effective generative method. It not only overcomes the limitations often associated with traditional AR models but also establishes a new level of performance that is highly competitive with the current state-of-the-art diffusion models.

Generation Time

To evaluate the generation efficiency of our model against existing methods, we conducted a speed benchmark. For each model, we generated 10,000 molecules using the respective official codebases and models pre-trained on the QM9 dataset. All experiments were performed on a single NVIDIA RTX 4090 GPU to ensure a fair comparison.

The total time taken to generate the full set of molecules is recorded for each model. As shown in Figure 4, our model demonstrates a highly competitive generation speed. It is significantly faster than diffusion-based models like Digress

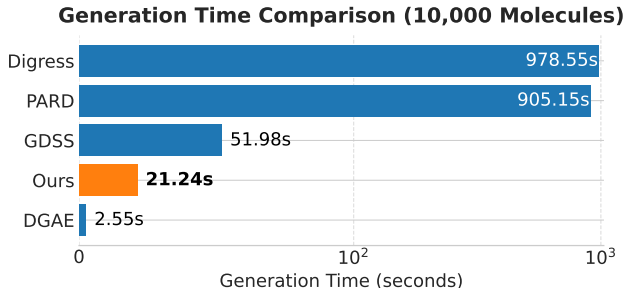


Figure 4: Comparison of generation time for sampling 10,000 molecules on the QM9 dataset. All models were benchmarked on an NVIDIA RTX 4090 GPU. The x-axis is on a logarithmic scale to better visualize the wide range of speeds. Our model shows a competitive generation time, significantly outperforming other diffusion-based methods.

(978.55s), GDSS (51.98s), and Autoregressive+Diffusion model like PARD(905.15s). While the autoregressive model DGAE is the fastest (2.55s), our approach (21.24s) achieves a practical and efficient generation time, striking a strong balance between speed and the quality afforded by our two-stage framework.

Conclusion

In this paper, we introduced the Graph VQ-Transformer (GVT), a two-stage framework for fast and high-quality molecular generation. Our core contribution is a novel Graph VQ-VAE that leverages canonical node ordering via RCM and a RoPE-enhanced decoder to achieve exceptionally high-fidelity discretization of molecular structures. By training an autoregressive Transformer on these superior discrete latents, GVT achieves near-perfect graph reconstruction and sets a new state-of-the-art on major benchmarks, including ZINC250k, MOSES, and GuacaMol. Its outperformance on key distribution metrics, such as FCD and KL Divergence, establishes that a well-designed discrete latent variable model can match and even exceed the performance of computationally intensive diffusion models, offering a powerful and efficient pathway for generative chemistry.

Acknowledgments

This work was supported by the National Natural Science Foundation of China [62071154].

References

- Boget, Y.; Gregorova, M.; and Kalousis, A. 2023. Discrete graph auto-encoder. *arXiv preprint arXiv:2306.07735*.
- Brown, N.; Fiscato, M.; Segler, M. H.; and Vaucher, A. C. 2019. GuacaMol: benchmarking models for de novo molecular design. *Journal of chemical information and modeling*, 59(3): 1096–1108.
- Cuthill, E.; and McKee, J. 1969. Reducing the bandwidth of sparse symmetric matrices. In *Proceedings of the 1969 24th national conference*, 157–172.
- De Cao, N.; and Kipf, T. 2018. MolGAN: An implicit generative model for small molecular graphs. *arXiv preprint arXiv:1805.11973*.
- Faez, F.; Ommi, Y.; Baghshah, M. S.; and Rabiee, H. R. 2021. Deep graph generators: A survey. *IEEE Access*, 9: 106675–106702.
- Irwin, J. J.; Sterling, T.; Mysinger, M. M.; Bolstad, E. S.; and Coleman, R. G. 2012. ZINC: a free tool to discover chemistry for biology. *Journal of chemical information and modeling*, 52(7): 1757–1768.
- Jin, W.; Barzilay, R.; and Jaakkola, T. 2018. Junction tree variational autoencoder for molecular graph generation. In *International conference on machine learning*, 2323–2332. PMLR.
- Jo, J.; Lee, S.; and Hwang, S. J. 2022. Score-based generative modeling of graphs via the system of stochastic differential equations. In *International conference on machine learning*, 10362–10383. PMLR.
- Landrum, G.; et al. 2016. Rdkit: Open-source cheminformatics software. 2016. URL <http://www.rdkit.org/>, <https://github.com/rdkit/rdkit>, 149(150): 650.
- Li, Y.; Zhang, L.; and Liu, Z. 2018. Multi-objective de novo drug design with conditional graph generative model. *Journal of cheminformatics*, 10: 1–24.
- Liao, R.; Li, Y.; Song, Y.; Wang, S.; Hamilton, W.; Duvenaud, D. K.; Urtasun, R.; and Zemel, R. 2019. Efficient graph generation with graph recurrent attention networks. *Advances in neural information processing systems*, 32.
- Luo, Y.; Yan, K.; and Ji, S. 2021. Graphdf: A discrete flow model for molecular graph generation. In *International conference on machine learning*, 7192–7203. PMLR.
- Nguyen, V. K.; Boget, Y.; Lavda, F.; and Kalousis, A. 2025. GLAD: Improving Latent Graph Generative Modeling with Simple Quantization. *Proceedings of the AAAI Conference on Artificial Intelligence*, 39(18): 19695–19702.
- Niu, C.; Song, Y.; Song, J.; Zhao, S.; Grover, A.; and Ermon, S. 2020. Permutation invariant graph generation via score-based generative modeling. In *International conference on artificial intelligence and statistics*, 4474–4484. PMLR.
- Oord, A. v. d.; Vinyals, O.; and Kavukcuoglu, K. 2018. Neural Discrete Representation Learning. *ArXiv:1711.00937 [cs]*.
- Polykovskiy, D.; Zhebrak, A.; Sanchez-Lengeling, B.; Golovanov, S.; Tatanov, O.; Belyaev, S.; Kurbanov, R.; Artamonov, A.; Aladinskiy, V.; Veselov, M.; et al. 2020. Molecular sets (MOSES): a benchmarking platform for molecular generation models. *Frontiers in pharmacology*, 11: 565644.
- Radford, A.; Wu, J.; Child, R.; Luan, D.; Amodei, D.; Sutskever, I.; et al. 2019. Language models are unsupervised multitask learners. *OpenAI blog*, 1(8): 9.
- Samanta, B.; De, A.; Jana, G.; Gómez, V.; Chattaraj, P.; Ganguly, N.; and Gomez-Rodriguez, M. 2020. NEVAE: A Deep Generative Model for Molecular Graphs. *Journal of Machine Learning Research*, 21(114): 1–33.
- Shi, C.; Xu, M.; Zhu, Z.; Zhang, W.; Zhang, M.; and Tang, J. 2020. Graphaf: a flow-based autoregressive model for molecular graph generation. *arXiv preprint arXiv:2001.09382*.
- Simonovsky, M.; and Komodakis, N. 2018. Graphvae: Towards generation of small graphs using variational autoencoders. In *International conference on artificial neural networks*, 412–422. Springer.
- Su, J.; Ahmed, M.; Lu, Y.; Pan, S.; Bo, W.; and Liu, Y. 2024. Roformer: Enhanced transformer with rotary position embedding. *Neurocomputing*, 568: 127063.
- Vignac, C.; Krawczuk, I.; Siraudin, A.; Wang, B.; Cevher, V.; and Frossard, P. 2022. Digress: Discrete denoising diffusion for graph generation. *arXiv preprint arXiv:2209.14734*.
- Wu, Z.; Ramsundar, B.; Feinberg, E. N.; Gomes, J.; Geniesse, C.; Pappu, A. S.; Leswing, K.; and Pande, V. 2018. MoleculeNet: a benchmark for molecular machine learning. *Chemical science*, 9(2): 513–530.
- Yan, Q.; Liang, Z.; Song, Y.; Liao, R.; and Wang, L. 2023. Swingnn: Rethinking permutation invariance in diffusion models for graph generation. *arXiv preprint arXiv:2307.01646*.
- Yang, L.; Tian, Y.; Xu, M.; Liu, Z.; Hong, S.; Qu, W.; Zhang, W.; Cui, B.; Zhang, M.; and Leskovec, J. 2023. Vqgraph: Rethinking graph representation space for bridging gnns and mlps. *arXiv preprint arXiv:2308.02117*.
- You, J.; Ying, R.; Ren, X.; Hamilton, W.; and Leskovec, J. 2018. Graphrnn: Generating realistic graphs with deep autoregressive models. In *International conference on machine learning*, 5708–5717. PMLR.
- Yun, S.; Jeong, M.; Kim, R.; Kang, J.; and Kim, H. J. 2019. Graph transformer networks. *Advances in neural information processing systems*, 32.
- Zhao, L.; Ding, X.; and Akoglu, L. 2024. Pard: Permutation-invariant autoregressive diffusion for graph generation. *Advances in Neural Information Processing Systems*, 37: 7156–7184.